Calculations of Swirl Combustors Using Joint Velocity–Scalar Probability Density Function Method

M. S. Anand∗and A. T. Hsu†
Allison Engine Company, Indianapolis, Indiana 46206
and
S. B. Pope‡
Cornell University, Ithaca, New York 14853

Calculations are reported for recirculating swirling reacting flows using a joint velocity–scalar probability density function (PDF) method. The PDF method offers significant advantages over conventional finite volume, Reynolds-average-based methods, especially for the computation of turbulent reacting flows. The PDF calculations reported here are based on a newly developed solution algorithm for elliptic flows, and on newly developed models for turbulent frequency and velocity that are simpler than those used in previously reported PDF calculations. Calculations are performed for two different gas-turbine-like swirl combustor flows for which detailed measurements are available. The computed results are in good agreement with experimental data.

Introduction

THE main advantages offered by the joint velocity–scalar probability density function (PDF) method for the computation of turbulent reacting flows are that the important processes such as convection by both mean and fluctuating velocities, the effect of turbulence fluctuations on complex multistep finite-rate reactions, and the effects of reaction/heat release on turbulence appear in closed form and need not be modeled.[1] In conventional Reynolds-averaged approaches, turbulent transport (convection by fluctuating velocities) is modeled using gradient diffusion assumptions, e.g., k–ε and Reynolds stress models. More importantly, the conventional models are incapable of accurately allowing for the effect of turbulent fluctuations of species and temperature on mean reaction rates for typical combustion reactions that involve multiple coupled reaction steps and highly nonlinear reaction rates. Further, the effects of heat release and the accompanying large density fluctuations on turbulence intensity and turbulent transport are not accurately modeled in conventional methods. Several previous studies reviewed by Pope[2] and more recent studies by Anand et al.[3,4] and Hsu et al.[5] have demonstrated the accuracy and advantages of the PDF method.

The ability to treat turbulent transport and reactions accurately is essential to the accurate predictions of heat release, pollutant formation, and other critical characteristics of combustors. Considerable progress has been made through ongoing work at Allison Engine Company in collaboration with Cornell University toward the development of the PDF method as the next-generation gas-turbine combustor design and analysis tool.[6] The present work is a significant step in that process.

The present work builds on several past studies, e.g., Refs. 3, 4, and 7–11. The study in Ref. 7 demonstrated the PDF method for elliptic recirculating flows. The PDF method was used in conjunction with a Reynolds-averaged finite volume method such that the Reynolds-averaged method supplied the mean pressure field and the turbulence time scale to the PDF method. The PDF method in turn supplied the Reynolds stresses to the Reynolds-averaged method, so that conventional turbulence models are avoided. The coupling was needed because the velocity–scalar PDF method used did not include information about the turbulence time scale. Although the mean pressure field could be determined from the mean velocity field, a robust algorithm was needed to solve the Poisson equation for pressure, which involves the evaluation of second derivatives of mean velocities and other terms with minimal statistical error. Such a pressure algorithm was developed by Anand et al.[8] and demonstrated for elliptic recirculating flows such as the flow over a backward-facing step. The time scale was still supplied externally to the PDF method in that study.

A model for the mean turbulence time scale, or rather for the mean turbulence frequency (reciprocal of the turbulence time scale), was developed and solved in conjunction with the PDF method by Anand et al.[9] Subsequently, a stochastic frequency model was developed by Pope et al.[10,11] With this model, the turbulence frequency is also considered as a random variable in the joint velocity–scalar-frequency PDF (or the joint velocity–scalar PDF where one of the scalars is the frequency), which would then contain the needed time-scale information. These models were used for computing swirling jet flows and swirling jet diffusion flames.[3,4] Because of the type of flows calculated, these computations were able to use boundary-layer assumptions for determining the pressure gradients and did not require the solution of the elliptic equation for pressure. All of the computations mentioned showed excellent comparison with detailed experimental data, including mean velocity and temperature and higher turbulent moments (compared up to fourth order).

The present study represents the first fully self-contained PDF calculations for elliptic flows and incorporates the elliptic-flow solution algorithm as well as the stochastic frequency model. However, with a view to making the method more robust, easier to implement, and affordable for complex multidimensional flows, a significantly different elliptic-flow algorithm (or pressure algorithm) has been developed and implemented. The models for turbulence frequency and for velocity have also been considerably simplified.

The newly developed method (elliptic algorithm and models) is validated against benchmark experimental data and the previous PDF solutions mentioned.

PDF Method: Modeling and Solution Algorithm

The joint PDF $f(V, \psi, \eta; x, t)$ at position x and time t is defined as the probability density of the simultaneous event $U(x, t) = V$, $\varphi(x, t) = \psi$, and $\omega(x, t) = \eta$, where U is the velocity vector, φ is a set of scalars, ω is the turbulence frequency, and V, ψ, and η are independent variables in the velocity–scalar-frequency space. Starting from the usual conservation equations for mass (continuity), momentum, scalar quantities, and turbulent frequency, the transport

equation for the joint PDF can be derived as described in Ref. 1. In this equation, the terms involving convection (mean and turbulent), reaction, body forces, and the mean pressure gradient effects (including the variable-density effects in those terms) appear in closed form. The terms representing the effects of viscous dissipation, fluctuating pressure gradient, molecular mixing of scalars, and production and dissipation of turbulence frequency need to be modeled. A Lagrangian viewpoint is adopted in modeling and solving the joint PDF equation. The modeled PDF transport equation is solved by the Monte Carlo technique.

In the Monte Carlo solution technique, notional particles, each representing a certain mass of fluid particles, are distributed throughout the solution domain overlaid by a spatial or computational grid. Each particle is attributed with values for its spatial position $x*$, velocity $U*$, scalar values $\varphi*$, and turbulence frequency $\omega*$. These values evolve according to the equations described next, which include modeled terms where needed. Starting from arbitrary initial conditions and specified boundary conditions, the particle values are marched in time steps that are a fraction of a characteristic time scale in the flow until a steady-state solution is reached. The solution of these evolution equations constitutes the solution of the PDF transport equation. Means (density-weighted) of any functions of the independent variables are determined by a sophisticated ensemble averaging procedure (cloud-in-cell estimate using bilinear basis functions) followed by smoothing using local linear least squares.[12] Additionally, time-averaging, with a low time constant initially and a higher one near convergence, is used for mean quantities to further reduce the statistical error.

Particle Evolution Equations

The increment $dx*$ in the position of a particle over an infinitesimal time interval dt during the time step is given by the exact equation

$$dx* = U* dt \tag{1}$$

This exact equation causes the mean and turbulent convection to be in closed form.

The model used for the increment in the particle velocity is a variant of the simple Langevin model and is described by

$$dU_i* = -\frac{1}{\rho*}\frac{\partial\langle P\rangle}{\partial x_i} - \left(\frac{1}{2}+\frac{3}{4}C_0\right)(U_i*-\langle U_i\rangle)\Omega\,dt + (C_0\Omega k)^{\frac{1}{2}}\,dW_i \tag{2}$$

where angled brackets denote (density-weighted or Favre) means, $\langle P(x*)\rangle$ is the mean pressure, $\langle U_i\rangle$ is the Eulerian mean velocity, k is the turbulent kinetic energy, Ω is the conditional mean turbulence frequency described later, $\rho*$ is the particle density, C_0 is a universal constant, and dW_i represents an isotropic Wiener random process. The first term in Eq. (2) exactly accounts for the acceleration due to mean pressure gradients including variable-density effects. The last two terms together model the effects of viscous dissipation and fluctuating pressure gradient.

The main difference between the current model and the simple Langevin model used previously, e.g., Refs. 3, 7–9, 13, and 14, is that the conditional mean frequency appears instead of the unconditional mean frequency $\langle\omega\rangle$. The conditional mean frequency is the above-average mean defined by[15]

$$\Omega = C_\Omega\langle\omega\mid\omega*\geq\langle\omega\rangle\rangle \tag{3}$$

i.e., it is proportional to the mean of the instantaneous frequencies that are greater than or equal to the unconditional mean frequency. In intermittent regions where both turbulent ($\omega > 0$) and nonturbulent ($\omega = 0$) fluid exist, the conditional mean frequency is representative of the frequency in the turbulent fluid, which is the appropriate quantity to use in modeling the turbulent process. As a consequence of its definition (3), Ω is larger than $\langle\omega\rangle$ in such regions. This facilitates the entrainment of nonturbulent particles without requiring additional modeling (see Ref. 15 for more details). The constant C_Ω (determined in terms of incomplete gamma functions) has the value 0.6893 and is specified so that $\Omega = \langle\omega\rangle$ in homogeneous turbulence.[15]

The value $C_0 = 2.1$ (determined in Ref. 13) has been used in previous studies for the simple Langevin model (2) that uses the unconditional mean frequency, e.g., Refs. 3, 7–9, 13, and 14. The appropriate value for the simple Langevin model using the conditional mean frequency (2) was determined in the present study to be $C_0 = 2.5$.

A new stochastic model for the evolution of the frequency of the particle $\omega*$, developed by Jayesh and Pope,[15] has been used in the present study. For the sake of brevity, the model is not presented here. Compared to the previous stochastic frequency model developed by Pope et al.,[10,11] the new model is easier to implement and is expected to be more robust. The new model includes the conditional mean frequency (3) and avoids the inclusion of an ad hoc term in the previous model to allow for intermittent regions. The evolution of the (unconditional) mean frequency, according to the model, is given by

$$\left\langle\frac{D\omega}{Dt}\right\rangle = C_1 S_{ij} S_{ij} - C_2\langle\omega\rangle^2 \tag{4}$$

where the left-hand side is the mean rate of change following the fluid, the first term on the right represents the production and the second term the decay of $\langle\omega\rangle$, and S_{ij} is the mean rate of strain, given by

$$S_{ij} = \frac{1}{2}\left(\frac{\partial\langle U_i\rangle}{\partial x_j} + \frac{\partial\langle U_j\rangle}{\partial x_i}\right) \tag{5}$$

Jayesh and Pope[15] suggest the values $C_1 = 0.08$ and $C_2 = 0.9$ for the constants in the frequency model. The same values are used in the present study.

The evolution of the αth species or scalar value of a computational particle is given by

$$d\varphi_\alpha* = S_\alpha(\varphi*)\,dt - C_\varphi(\varphi_\alpha* - \langle\varphi_\alpha\rangle)\Omega\,dt \tag{6}$$

where $S_\alpha(\varphi*)$ is the reaction rate for the species φ_α as a function of the instantaneous composition $\varphi*$. Therefore, given the reaction rate (determined by the thermochemistry used), the treatment of reaction and the turbulence chemistry interactions are in closed form. The second term in Eq. (6) represents a simple relaxation-to-mean model for molecular mixing of scalars proposed by Dopazo[16] and known as the interaction by exchange with the mean model. The value of the constant C_φ is typically in the range 1.5–2.0. The value $C_\varphi = 1.5$ is used in the present study.

Additional comparative discussion of the models used in some of the previous studies and the present study and the relationships between the constants for the different models can be found in Ref. 7. All of the models presented in Ref. 7 have performed satisfactorily and have produced good agreement with experimental data for a variety of flows using the same set of values of model constants for the respective models. The choice of the models used in the present study is motivated by the applicability and ease of implementation of the models for computations of complex multidimensional flows.

The values of the model constants in the present study ($C_0 = 2.5$, $C_1 = 0.08$, $C_2 = 0.9$, and $C_\varphi = 1.5$) were the same for all of the flows computed. A parametric study varying the constants over a range of values ($C_0 \approx 2.1$–3.5, $C_1 \approx 0.04$–0.08, $C_2 \approx 0.7$–0.9, and $C_\varphi \approx 1.0$–2.0) showed that whereas the results were not overly sensitive to the values of the constants in the range studied, the choice produced the best overall agreement with the data.

The time increment Δt for each step is chosen to be a fraction ($=0.1$) of the minimum of 1) the reciprocal of the maximum mean turbulence frequency in the computational domain and 2) the minimum characteristic time for any particle to cross a computational cell, based on the mean and variance of velocity in the cell. All of the particles in the computation are marched with the same time increment. The particle evolution equations are integrated over the time step with an accuracy of second order or better.

Note that the models described for velocity, frequency, and scalar mixing are all being used in the joint PDF method for the first time to compute general (inhomogeneous, swirling, recirculating) turbulent reacting flows. Thus, the present study serves to validate the elliptic-flow algorithm as well as the models used.

Elliptic-Flow Algorithm (Position, Velocity, and Pressure Correction)

The main purpose of the elliptic flow algorithm is to determine the mean pressure field to be used in the velocity equation (2) while

ensuring that the mean conservation equations for mass and momentum are satisfied. The elliptic-flow algorithm, newly developed by Pope,[17] is used in the present study. The algorithm performs a velocity correction to satisfy mean mass conservation and determines a mean pressure correction on every step starting from arbitrary initial conditions. Variance reduction techniques are applied (i.e., turbulent processes such as mixing, viscous dissipation, etc., are performed on subensembles in such a way that the subensemble means are not changed) so that mean momentum conservation is also maintained. In addition, a correction to the position of the particles is made to ensure that the consistency condition for particle methods, namely that the volume associated with a subensemble of particles should equal the geometric volume occupied by the particles, is satisfied. For statistically stationary flows, a steady state is achieved in which the mean values of these corrections tend to zero (and the variance decreases as the number of particles increases).

In the algorithm, a velocity correction potential Φ is determined such that after adding the velocity correction

$$\delta U = -(1/\langle \rho \rangle)\nabla \Phi \qquad (7)$$

the corrected velocity field satisfies the continuity equation ($\langle \rho \rangle$ is the mean density of the fluid). When the velocity increment is determined by Eq. (7) for a time step Δt, it is equivalent to the effect of a mean pressure correction

$$\delta \langle P \rangle = \Phi/\Delta t \qquad (8)$$

The Poisson equation for the velocity correction potential is set up and solved using a bilinear-basis-function representation for calculating mean quantities. Thus, the mean pressure field is not determined directly from the solution of the Poisson equation. However, any error in the mean pressure field is compensated by the velocity correction, i.e., the potential Φ is such the total effect of the correct pressure should be felt.

In contrast, the pressure algorithm developed and used by Anand et al.[8] solves for the Poisson equation for pressure as well as for the velocity correction potential. However, because the Poisson equation involves second derivatives of mean velocities, it is necessary to determine the mean velocity field to a high degree of accuracy. Hence bidirectional cross-validated cubic splines are used to determine means in that algorithm that can be computationally expensive. The current algorithm is expected to be less expensive and more robust. The more important advantage is that it is easier to extend the current algorithm to irregular geometries (body-fitted grids) and to three-dimensional flow calculations.

Thermochemistry

Hydrogen and methane flames are studied in the present work. A fast equilibrium chemistry model is used for the hydrogen flame calculations because the time scale for hydrogen–air reaction is very small compared to the turbulent time scale. For the hydrogen case, the only scalar variable in the calculations is the mixture fraction. Temperature is also included but is needed for output only. The mixture fraction is a conserved variable (reaction rate is zero). The density and temperature are determined as equilibrium properties from the mixture fraction.

For methane flame calculations, a general two-step chemistry due to Westbrook and Dryer[18] for saturated hydrocarbon fuels is used. The two steps are

$$C_nH_m + [(n/2) + (m/4)]O_2 = nCO + (m/2)H_2O \qquad (9)$$

$$CO + \tfrac{1}{2}O_2 = CO_2 \qquad (10)$$
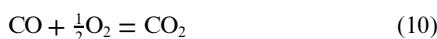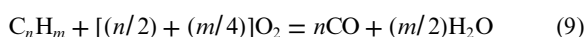
In addition to the mixture fraction, two more scalar variables, namely the mass fractions of carbon dioxide and water vapor, are included in the PDF calculations. The temperature and density are determined as functions of these three scalar variables.

For both the fast chemistry and the two-step chemistry models, lookup tables were created to reduce the CPU requirements of the calculations. In the case of the fast chemistry, a one-dimensional table is created, and for the two-step chemistry, a three-dimensional table is generated. For the two-step chemistry calculations, the table is generated for a given specific time increment Δt used by the flow

calculations ($\Delta t = 2.5 \times 10^{-5}$ s in the present calculations). In the table generation processes, the NASA CEC thermal data were used to calculate the variable specific heats and the temperature.

Results and Discussion

The present PDF method was applied to the (constant-density) flow over a backward-facing step previously calculated by Anand et al.,[8] for which measurements have been reported.[19] As before, the results (not presented here) were in excellent agreement with data for the reattachment length, mean velocities, and up to third-order turbulent correlations measured.

Results are presented for two laboratory swirl combustor configurations that have the essential flow features of gas turbine combustors, namely swirl, recirculation, large velocity gradients, turbulence, and combustion. The experiments were conducted by researchers at the University of Dayton Research Institute at the Wright–Patterson Air Force Base, Dayton, Ohio. The velocity measurements were made using a three-component laser Doppler velocimeter (LDV), and the temperature measurements were made using coherent anti-Stokes Raman spectroscopy (CARS).

Swirling Hydrogen Diffusion Flame

Figure 1 shows the schematic of the swirling jet diffusion flame combustor configuration. The test case considered had a central fuel (hydrogen) jet bulk velocity of 100 m/s, a swirling air bulk velocity of 20 m/s, and a nonswirling coflow air velocity of 4 m/s. The swirler vane angle was 30 deg, and the swirl number for the swirling jet, calculated from the measured velocities, was 0.382. Detailed measurements for mean velocities and turbulent correlations up to fourth order are reported (see references listed in Ref. 4) at several downstream locations starting from the axial location $x = 1.5$ mm from the nozzle. Although no species measurements were made, the mean and variance of the temperature are reported at the same locations.

The flow was previously calculated by Anand et al.[4] using a joint PDF method. Because the flow is primarily parabolic (with no recirculation), the PDF solution algorithm was based on boundary-layer assumptions with extensions for swirling flows. The method also used more sophisticated models, namely the stochastic frequency model of Pope[11] in conjunction with the refined Langevin model for velocity,[11] in which the instantaneous particle frequency rather
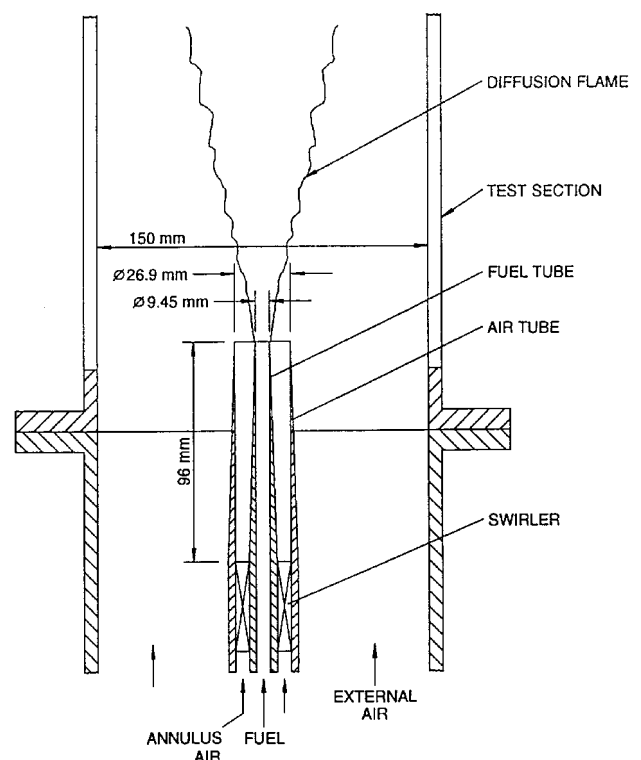

Fig. 1 Schematic of the hydrogen swirling jet diffusion flame configuration.

than a mean frequency is used in the random term shown in Eq. (2), along with a resulting additional drift term. The reason for calculating the flow with the present method is not only to validate the method and the model but also to assess whether the elliptic flow algorithm can better resolve the flow in regions where boundary-layer assumptions, e.g., neglect of axial gradients, are questionable.

The inlet boundary conditions for the present computations were taken, as before, from experimental data (see Ref. 4 for details). The initial transverse profiles within the solution domain were set to be the same as at the inlet plane. The computational domain extended from the inlet to an x/D of approximately 30. The computations were performed on an IBM RS6000/370 using a nonuniform grid (31 along $x \times 61$ along the radius r) with about 190 particles per cell. Increasing the nominal number of particles per cell to 290 produced nearly the same computed results, showing that the number of particles used is sufficient. For a given total number of particles, the statistical error in the calculations of the means (and more severely for gradients of means) increases with a decrease in grid size, i.e., with an increase in the number of grids, whereas a large grid size results in loss of resolution.[12] Hence, a moderate grid size consistent with the needed resolution in the flow is chosen to minimize statistical errors. Work is in progress to systematically quantify the effects of the number of particles and grid size on the computed mean values and on the solution of the particle evolution equations and the mean-pressure-related equations where the means are used.[20]

In the figures to be presented for this case, the measured mean axial velocity on the centerline at the nozzle exit, $\langle U \rangle_{0c}$, which is 130.3 m/s in this case, is used to normalize the velocity statistics. The axial and radial distances are normalized by the nozzle diameter $D (=9.45 \text{ mm})$ and nozzle radius $R (= D/2)$, respectively. The temperature results are normalized by the stoichiometric temperature $T_{st} (=2377 \text{ K})$. For the experimental data presented, the open squares represent data conditioned on the inner fuel jet, the solid circles represent data conditioned on the swirling air jet, and the inverted triangles represent the data conditioned on the outer coflow air.

Calculations were performed for 2000 time steps for both the hydrogen and the methane (presented in the next subsection) combustors. In real time this corresponded, for both cases, to approximately six times the characteristic mean time scale, defined as the time that a fluid particle with constant velocity $\langle U \rangle_{0c}$ would take to traverse from the inlet to the exit of the solution domain. Figure 2 shows the convergence history for the normalized mean axial velocity at the indicated monitoring locations for the hydrogen and the methane combustors ($\langle U \rangle_{0c} = 21.6$ m/s for the methane case). Figure 2 shows that the solutions have converged and the steady state has been reached. As expected, the computed values at the far-field location relative to the inlet nozzle ($x/D = 10, r/R = 4$) respond slowly compared to the near-nozzle location ($x/D = 1, r/R = 0.7$), where typically oscillations in the values are seen during the initial (first few hundred) steps before the solution settles down and reaches a steady state.

Figure 3 shows the radial profiles of the normalized mean axial velocity $\langle U \rangle$ at different downstream locations compared against data. The measurements are conditional on the origin of the fluid and are made by seeding (for LDV) each of the jets (fuel, annulus, and coflow) individually. Differences in the velocity statistics for each of
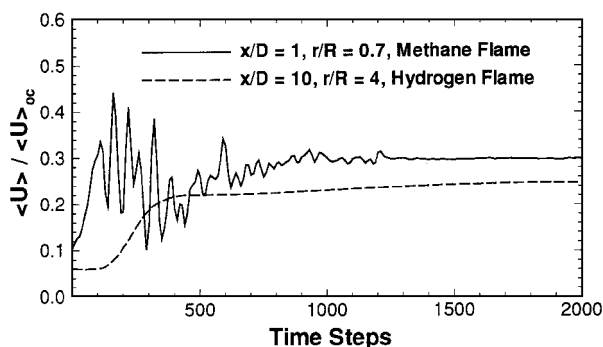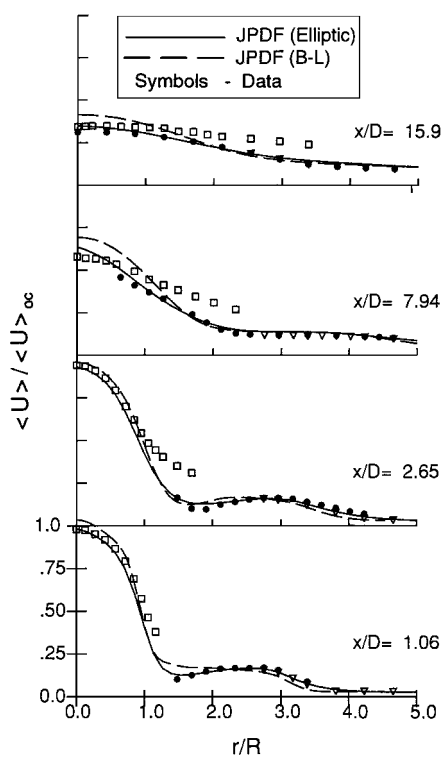
Fig. 3   Computed mean axial velocity profiles compared against data for the hydrogen flame.

the jets can be seen in the data. The PDF method can calculate these conditional values without requiring additional modeling, and such calculations have been presented in Refs. 3 and 4. However, in the present study, only the unconditional quantities are calculated and compared against data. The present joint PDF (JPDF) results from the elliptic algorithm (solid lines) are also compared against JPDF results from the boundary-layer (B-L) algorithm (dashed lines).[4] Figure 3 shows that the present results are in excellent agreement with data at all stations. Also, the present calculations are in better agreement with data than the boundary-layer results not only with respect to the overall spreading but also in the near-nozzle region ($x/D = 1.06$ and 2.65), where the flow is tending toward recirculation (near $r/R = 1.5$) and the boundary-layer approximations are inaccurate.

Similar observations can be made for the swirl velocity results presented in Fig. 4. Although the boundary-layer calculations are in good agreement with the data, the present calculations show better agreement.

The profiles of mean (Reynolds-averaged) temperature $\bar{T}$ presented in Fig. 5 show that the transport and mixing of the fuel is well calculated in the present study, resulting in good agreement with the temperature data. (The Reynolds-averaged temperature is plotted because CARS measurements are closer to Reynolds-averaged values than to density-weighted values.[4]) The present results are better than the boundary-layer results at the downstream locations, but near the nozzle, e.g., $x/D = 2.65$, the present results show a lower peak and a greater spread than the data and the boundary-layer results show. The measured temperatures near the centerline at $x/D = 15.6$ are higher than the predicted values because the CARS measurements rely on the presence of nitrogen molecules,[4] and the data at locations where there is significant probability of presence of both burnt and unburnt fuel are biased toward the hotter nitrogen-containing combustion products and do not take into account the colder hydrogen fuel parcels. Results for the temperature variance from both the methods (not shown here) were overall in good agreement with data, although some differences consistent with their mean temperature profiles were observed. This agreement has to be viewed in the context of the large discrepancies between temperature data and results from conventional models reported in Ref. 5.

Profiles for turbulent kinetic energy presented in Fig. 6 show that both the calculations are in good agreement with data in the
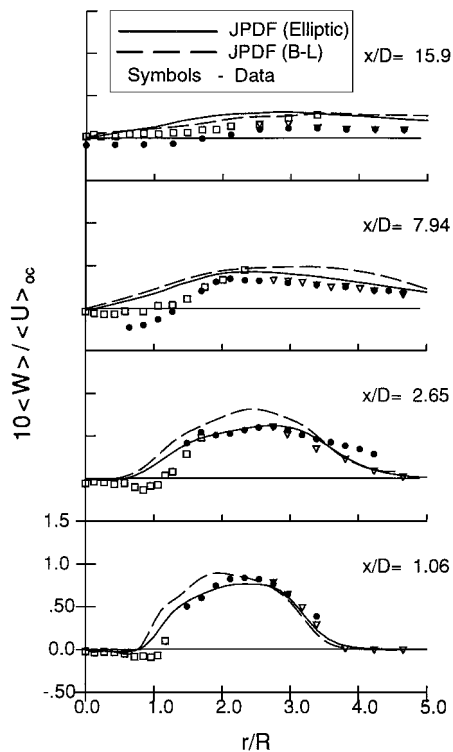
Fig. 2   Convergence history for the hydrogen and methane flame computations.

Fig. 4   Computed mean swirl velocity profiles compared against data for the hydrogen flame.
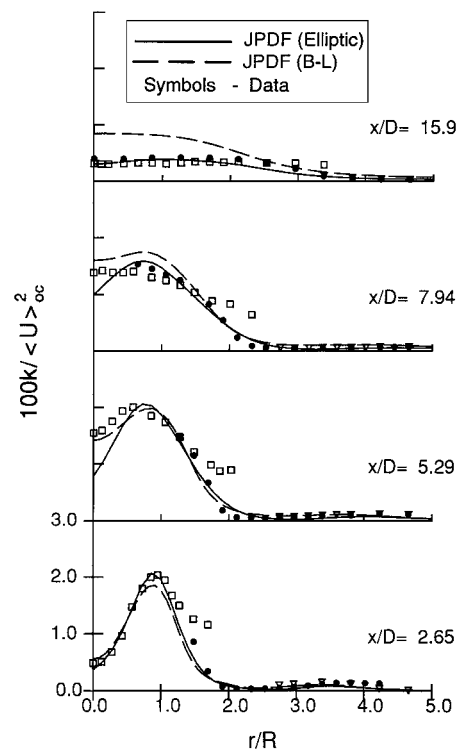

Fig. 6   Computed turbulent kinetic energy profiles compared against data for the hydrogen flame.
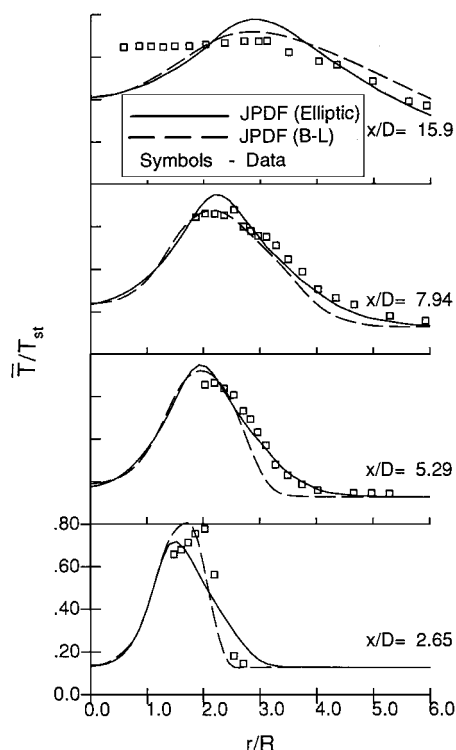

Fig. 5   Computed mean temperature profiles compared against data for the hydrogen flame.

Fig. 7   Computed profiles of higher-order turbulent correlations compared against data for the hydrogen flame.

region up to $x/D = 5.29$, whereas the boundary-layer calculations overpredict the kinetic energy at downstream locations, which is consistent with the lack of spreading in the mean velocity profiles. Sample results from the present calculations for third- and fourth-order turbulent correlations, presented in Fig. 7, are in good agreement with data.

Overall, the results are in very good agreement with data and are as good as or better than those obtained with the boundary-layer calculations.
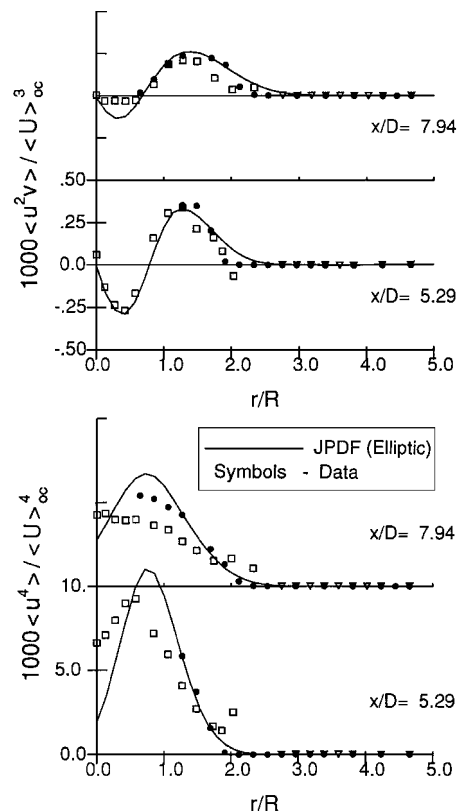
Methane Step-Swirl Combustor

The step-swirl combustor shown in Fig. 8 is an extension of the jet diffusion flame combustor (Fig. 1) and is closer to a practical gas turbine combustor. It consists of a central air jet (20-mm diam) surrounded by an annular fuel tube (29-mm o.d.), which is again surrounded by a swirling air jet (40-mm o.d., taken to be the characteristic diameter D). Measurements for this case are reported in Ref. 21. For the case considered here, the inner air jet was
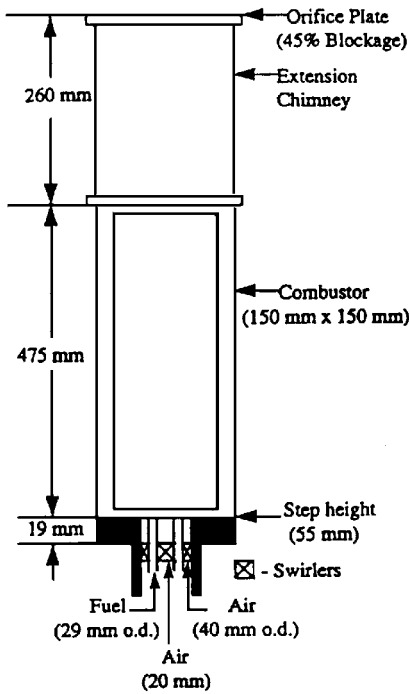
Fig. 8   Schematic of the step-swirl combustor. The fuel used is methane.

Fig. 9   Computed mean axial velocity profiles (lines) compared against data (symbols) for the methane flame.

nonswirling and the outer air had a 30-deg-vane-angle swirler. The bulk velocity for the inner air, fuel, and outer air jets are 14.4, 2.5, and 8.6 m/s, respectively.

The velocity data reported for this combustor are also conditional velocities. Unfortunately, the authors[21] were unable to measure the velocities conditional on the outer air jet because of practical difficulties such as the LDV seed particles striking the optical windows and clogging them up. The outer swirling flow has a major effect on the development of the flow, and it is crucial to have accurate inlet conditions to simulate the flow accurately. The computations also show high sensitivity to the inlet profiles, especially in that the comparison with data is made in the region $x/D < 2$ where measurements were made. In the present study, the inflow velocity profiles had to be reconstructed on the basis of existing experimental data at $x = 3$ mm ($x/D = 0.075$) and the overall mass flow rates through the different streams.

The initial transverse profiles within the solution domain were set to be the same as at the inlet plane. The solution domain extended from the inlet to $x/D = 4.5$. The computations were performed using a nonuniform 41×41 grid using 200 particles per cell. The computations were made for 2000 steps, and convergence was achieved in most of the flowfield by about 1500 steps. The results are presented in Figs. 9–14. The values used for normalization in the figures are $\langle U \rangle_{0c} = 21.6$ m/s, $T_{st} = 2272$ K, $D = 40$ mm, and $R = D/2$. For the experimental data presented, the solid symbols represent data conditioned on the inner air jet and the open symbols represent data conditioned on the fuel jet.

The profiles of mean axial velocity $\langle U \rangle$ presented in Fig. 9 show that the calculations capture the overall flow features well. Although the recirculation is well predicted, the location and radial extent of the recirculation zone, which are very sensitive to the inlet mean radial and swirl velocities assumed for the outer swirling jet, are underpredicted.

The profiles of mean radial velocity $\langle V \rangle$, in Fig. 10, show the expected trends, although data are not available in the critical regions where the largest radial velocities are present. Note that computed results are unconditional and are expected to be lower than the fuel conditioned radial velocity at the outer edge of the fuel jet as seen at $x/D = 0.5$. Figure 11 shows that the mean swirl (or tangential) velocity $\langle W \rangle$ is well predicted in terms of both the peak location and the decay downstream.

The mean temperature profiles presented in Fig. 12 predict the shapes of the measured profiles well and for the most part agree in magnitude with the data. The profile of the fuel mass fraction at the
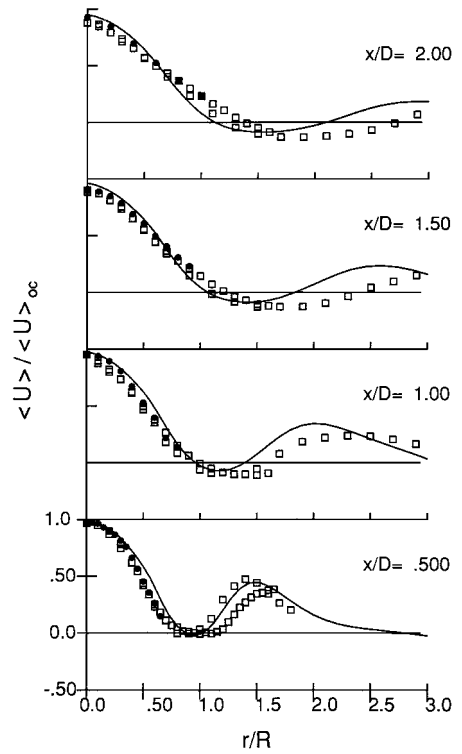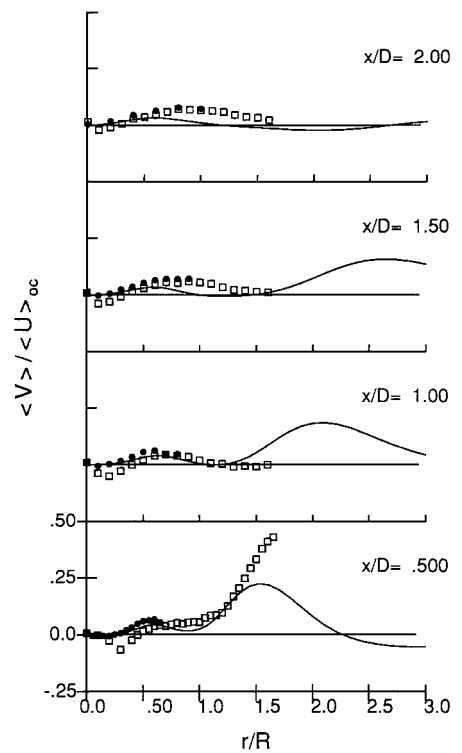

Fig. 10   Computed mean radial velocity profiles (lines) compared against data (symbols) for the methane flame.

inlet significantly influences the temperature distribution at the near-nozzle locations at which comparisons are being made. Although the fuel tube only supplies fuel, considerable mixing takes place even as the fuel is leaving the fuel tube, and an assumption of a plug flow profile leads to a much worse comparison with temperature than does the smooth but sharply peaked profile assumed for the computations shown.

The profiles of turbulent kinetic energy and a fourth-order turbulent correlation shown in Figs. 13 and 14, respectively, are in
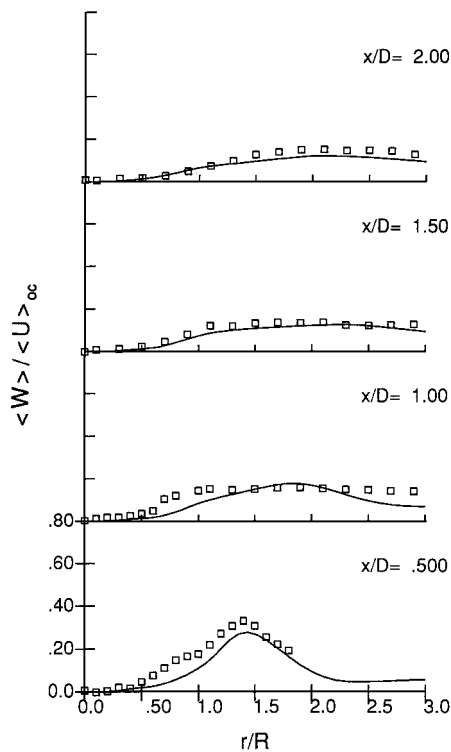
Fig. 11 Computed mean swirl velocity profiles (lines) compared against data (symbols) for the methane flame.
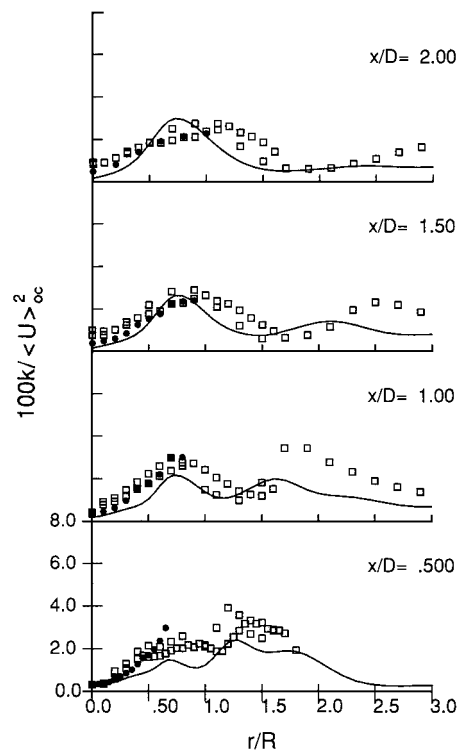

Fig. 13 Computed turbulent kinetic energy profiles (lines) compared against data (symbols) for the methane flame.
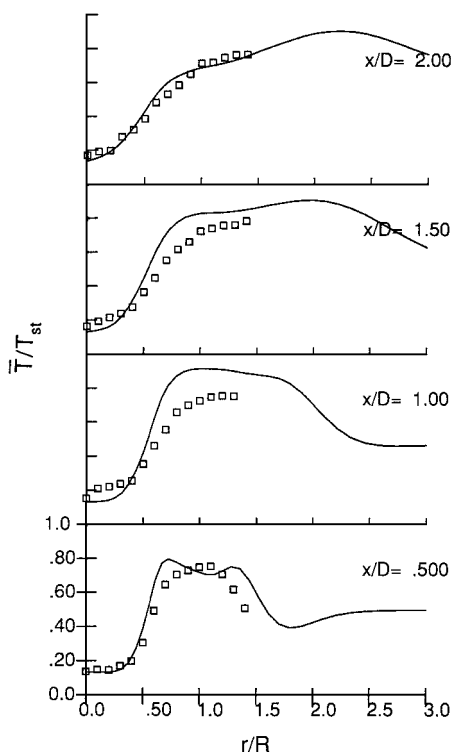

Fig. 12 Computed mean temperature profiles (lines) compared against data (symbols) for the methane flame.

Fig. 14 Computed profiles of fourth moment of axial velocity (lines) compared against data (symbols) for the methane flame.

reasonably good agreement with data. Overall, the results are in good agreement with the data for all of the quantities, considering the uncertainty in the inlet conditions.

The results for the hydrogen and methane cases have validated the new models and the elliptic-flow algorithm used. The calculations represent the first quantitative results from the new code incorporating the algorithm and models. The results compare very well with the detailed data from practical combustors.
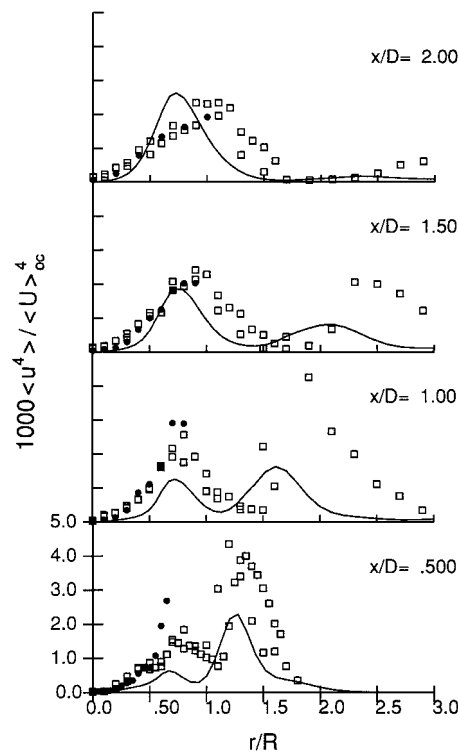
Concluding Remarks

Computations using the joint PDF approach have been reported for two swirl combustor configurations. The study uses a newly developed solution algorithm for elliptic flows and new simplified models for velocity and turbulence frequency. The methane combustor calculations represent the first fully self-contained joint PDF calculations for elliptic reacting flows. The results for both combustors are in good agreement with the data. The study serves to further validate the joint PDF method and the models and is a significant step in the development of a PDF-based combustor design system.

The ability of the joint PDF method to calculate accurately the mean and turbulent velocity fields, scalar transport, and temperature using multistep finite-rate chemistry offers significant advantages for its use in the design of current and future high-performance and low-emission gas turbine combustors.

The present results are compared against calculations using the scalar PDF method (in which the joint PDF of only the scalars is considered) and other conventional turbulent combustion models in an accompanying paper.[5] The study demonstrates the advantages and the superior accuracy of PDF methods, in particular the joint velocity–scalar PDF method.

Acknowledgments

References

[1]Pope, S. B., "PDF Methods for Turbulent Reacting Flows," *Progress in Energy and Combustion Science*, Vol. 11, 1985, pp. 119–192.

[2]Pope, S. B., "Computations of Turbulent Combustion: Progress and Challenges" (Invited Plenary Lecture), *Twenty-Third Symposium (International) on Combustion*, Combustion Inst., Pittsburgh, PA, 1990, pp. 591–612.

[3]Anand, M. S., Pope, S. B., and Mongia, H. C., "PDF Calculations for Swirling Flows," AIAA Paper 93-0106, Jan. 1993; also *AIAA Journal* (to be published).

[4]Anand, M. S., Takahashi, F., Vangsness, M. D., Durbin, M. D., and Schmoll, W. J., "An Experimental and Computational Study of Swirling Hydrogen Jet Diffusion Flames," *Journal of Engineering for Gas Turbines and Power*, Vol. 119, April 1997, pp. 305–314; also ASME Paper 95-GT-307, June 1995.

[5]Hsu, A. T., Anand, M. S., and Razdan, M. K., "An Assessment of PDF Versus Finite Volume Methods for Turbulent Reacting Flows," AIAA Paper 96-0523, Jan. 1996; also *Journal of Propulsion and Power* (to be published).

[6]Anand, M. S., Pope, S. B., and Razdan, M. K., "Combustor Design Model Evaluation," U.S. Air Force Wright Lab., Rept. WL-TR-96-2059, Wright–Patterson AFB, OH, April 1996.

[7]Anand, M. S., Pope, S. B., and Mongia, H. C., "A PDF Method for Turbulent Recirculating Flows," *Turbulent Reactive Flows*, Vol. 40, Lecture Notes in Engineering, Springer–Verlag, New York, 1989, pp. 672–693.

[8]Anand, M. S., Pope, S. B., and Mongia, H. C., "Pressure Algorithm for Elliptic Flow Calculations with the PDF Method," *CFD Symposium on Aeropropulsion*, NASA CP-3078, 1990, pp. 347–362.

[9]Anand, M. S., Pope, S. B., and Mongia, H. C., "Calculations of Axisymmetric Turbulent Jets by the PDF Method," *Seventh Symposium on Turbulent Shear Flows*, Stanford Univ., Stanford, CA, 1989, pp. 3.3.1–3.3.6.

[10]Pope, S. B., and Chen, Y. L., "The Velocity–Dissipation Probability Density Function Model for Turbulent Flows," *Physics of Fluids A*, Vol. 2, No. 8, 1990, pp. 1437–1449.

[11]Pope, S. B., "Application of the Velocity–Dissipation Probability Density Function Model to Inhomogeneous Turbulent Flows," *Physics of Fluids A*, Vol. 3, No. 8, 1991, pp. 1947–1957.

[12]Dreeben, T. D., and Pope, S. B., "Nonparametric Estimation of Mean Fields with Application to Particle Methods for Turbulent Flows," Sibley School of Mechanical and Aerospace Engineering, Cornell Univ., FDA 92-13, Ithaca, NY, Nov. 1992.

[13]Anand, M. S., and Pope, S. B., "Diffusion Behind a Line Source in Grid Turbulence," *Turbulent Shear Flows 4*, edited by L. J. S. Bradbury, F. Durst, B. E. Launder, F. W. Schmidt, and J. H. Whitelaw, Springer–Verlag, New York, 1985, pp. 46–61.

[14]Haworth, D. C., and Pope, S. B., "A PDF Modeling Study of Self-Similar Turbulent Shear Flows," *Physics of Fluids*, Vol. 30, 1987, pp. 1026–1044.

[15]Jayesh, and Pope, S. B., "Stochastic Model for Turbulent Frequency," Sibley School of Mechanical and Aerospace Engineering, Cornell Univ., Rept. FDA 95-05, Ithaca, NY, Oct. 1995.

[16]Dopazo, C., *Physics of Fluids*, Vol. 18, 1975, p. 397.

[17]Pope, S. B., "Position, Velocity, and Pressure Correction Algorithm for Particle Method Solution of the PDF Transport Equations," Sibley School of Mechanical and Aerospace Engineering, Cornell Univ., Rept. FDA 95-06, Ithaca, NY, Oct. 1995.

[18]Westbrook, C. K., and Dryer, F. L., "Simplified Reaction Mechanisms for the Oxidation of Hydrocarbon Fuels in Flames," *Combustion Science and Technology*, Vol. 27, 1981, pp. 31–43.

[19]Pronchick, S. W., and Kline, S. J., "An Experimental Investigation of the Structure of Turbulent Reattaching Flow Behind a Backward-Facing Step," Dept. of Mechanical Engineering, Stanford Univ., Rept. MD-42, Stanford, CA, 1983.

[20]Xu, J., and Pope, S. B., "Sources of Bias in Particle-Mesh Methods for PDF Models for Turbulent Flows," Sibley School of Mechanical and Aerospace Engineering, Cornell Univ., FDA 97-01, Ithaca, NY, Jan. 1997.

[21]Durbin, M. D., Vangsness, M. D., Ballal, D. R., and Katta, S. R., "Study of Flame Stability in a Step Swirl Combustor," American Society of Mechanical Engineers, Paper 95-GT-111, June 1995.

K. Kailasanath
Associate Editor